# Unlocking Spectral Efficiency in Intensity Modulation and Direct Detection Systems

Dobroslav Tsonev, *Member, IEEE*, Stefan Videv, and Harald Haas, *Member, IEEE*

***Abstract*—A number of inherently unipolar orthogonal frequency division multiplexing (OFDM) modulation schemes have been introduced recently in an attempt to improve the energy efficiency of OFDM-based intensity modulation and direct detection (IM/DD) systems. All such algorithms, including asymmetrically clipped optical OFDM (ACO-OFDM), pulse-amplitude-modulated discrete multitone modulation (PAM-DMT) and unipolar orthogonal frequency division multiplexing (U-OFDM), experience an inherent loss in spectral efficiency caused by the restrictions imposed on the OFDM frame structure required for the generation of a unipolar signal. The current paper presents a modified modulation approach, termed enhanced U-OFDM (eU-OFDM), which compensates the spectral efficiency loss in U-OFDM. At the same time, it still allows for the generation of an inherently unipolar modulation signal that achieves better performance in terms of both electrical power and optical power dissipation compared to the conventional state-of-the-art technique direct current (DC)-biased optical OFDM (DCO-OFDM). To the best of the authors' knowledge, the current work also presents the first experimental proof-of-concept demonstration of both U-OFDM and eU-OFDM, and clearly demonstrates the significant energy advantages that these two schemes can introduce in an optical wireless communications (OWC) system.**

***Index Terms*—Optical wireless communication (OWC), orthogonal frequency division multiplexing (OFDM), optical modulation, intensity modulation and direct detection (IM/DD).**

## I. Introduction

DATA throughput in wireless communication networks is increasing exponentially. By 2017, it is expected that traffic demands in mobile networks will be more than 11 Exabytes per month [1]. Despite the significant technological progress in cellular communications over recent years, it is anticipated that meeting the future data rate demands will be challenging [2]. This stems from the fact that the radio frequency (RF) spectrum below 10 GHz, conventionally used for wireless communication, is insufficient to meet future demands. A potential solution to the spectrum crisis is the migration of wireless communication into new and largely under-utilized regions of the electromagnetic spectrum such as the millimetre, the infrared and the visible light wavelengths. Optical wireless communication is a very promising candidate for providing a complementary alternative to RF communication. The optical spectrum offers hundreds of THz unregulated bandwidth. In addition, optical radiation does not interfere with the operation of sensitive electronic systems. Furthermore, the existing lighting infrastructure could be reused which could significantly simplify the integration of OWC into future heterogeneous wireless networks [3]. Moreover, OWC systems have the potential to deliver significant energy savings when successfully serving the dual purpose of communication and illumination.

Commercially available light emitting diodes (LEDs) and photodiodes (PDs) are potential low-cost front-end devices for use in OWC [3]. Off-the-shelf LEDs emit incoherent light and, therefore, they can reliably convey information only in the intensity of the light signal. The phase and the amplitude of the electromagnetic wave cannot be modulated or detected with LEDs and PDs. Hence, an OWC system using such front-end devices can only be realised as an IM/DD system. This means that conventional RF modulation schemes cannot always be straightforwardly applied. Some techniques such as on-off keying (OOK), pulse-position modulation (PPM), and $M$-ary pulse-amplitude modulation ($M$-PAM), which generate a real signal, are relatively straightforward to implement.

The limited bandwidth of a communication channel leads to inter-symbol interference (ISI) at high data rates. The modulation bandwidth over which the frequency response of most commercially available LEDs can be considered flat is around 2–20 MHz [4]–[6]. This implies that high-speed OWC is likely to require modulation rates well beyond the 3-dB modulation bandwidth of the front-end components and an appropriate equalisation technique at the receiver. Therefore, OFDM becomes a very appealing option for a modulation scheme. It enables cost effective equalisation with single-tap equalisers in the frequency domain, as well as adaptive data and energy loading in different frequency regions depending on the communication channel properties. This results in an optimal utilisation of the available communication resources. In fact, the fastest data rates reported so far in the field of visible light communications (VLC)—over 3 Gb/s for a single-colour LED [6]—have all been achieved with the use of OFDM [4]–[6]. At the medium access control (MAC) level, OFDM provides a straightforward multiple access scheme, which is less straightforward to implement in OOK, PPM and $M$-PAM.

In practical implementations, OFDM is realised by applying an inverse fast Fourier transform (IFFT) operation on a block of

Manuscript received June 6, 2014; revised October 16, 2014 and March 10, 2015; accepted April 13, 2015. Date of publication May 13, 2015; date of current version August 17, 2015. This work was supported by the UK Engineering and Physical Sciences Research Council under Grant EP/K008757/1. Parts of this work were presented at the IEEE International Conference on Communications, 2014.

The authors are with the Institute for Digital Communications, Li-Fi R&D Centre, University of Edinburgh, Edinburgh EH9 3JL, UK (e-mail: d.tsonev@ed.ac.uk; s.videv@ed.ac.uk; h.haas@ed.ac.uk).

Color versions of one or more of the figures in this paper are available online at http://ieeexplore.ieee.org.

Digital Object Identifier 10.1109/JSAC.2015.2432530

symbols from a conventional digital modulation scheme such as $M$-ary quadrature amplitude modulation ($M$-QAM). This procedure effectively maps the different $M$-QAM symbols to different subcarriers/subbands in the frequency domain of the resulting time-domain signal. The IFFT operation, however, generates complex-valued time-domain samples, while intensity modulation requires real non-negative signals. Hence, the OFDM signal has to be modified before it can be applied to an IM/DD system. A real time-domain signal can be obtained by imposing a Hermitian symmetry constraint to the information block which is processed in the IFFT operation [7], [8]. The resulting real time-domain samples, however, are bipolar.

There are a number of different techniques for generating a unipolar OFDM signal. A straightforward method, proven in practice [4]–[6], is to introduce a positive DC bias level around which the bipolar information signal can be applied. This approach is referred to as DCO-OFDM. The DC bias significantly increases the energy dissipation of the transmitter front-end. For example, according to Monte Carlo simulations conducted, a 4-QAM DCO-OFDM information signal requires a minimum bias which results in an electrical power dissipation penalty of about 6–7 dB, compared to a bipolar OFDM signal. For higher modulation orders, the power penalty increases further. As a result, research has been dedicated to exploring alternative methods for the generation of unipolar OFDM-based signals. Unipolar modulation schemes such as ACO-OFDM [9], PAM-DMT [10], U-OFDM [11] and Flip-OFDM [12] have been developed. These techniques exploit the properties of the fast Fourier transform (FFT) and the structure of the OFDM frame in order to generate an inherently unipolar signal, i.e., a signal that does not require any DC-biasing to be made unipolar and can be directly applied to an IM/DD system. Note that all four inherently unipolar approaches achieve equivalent performance in an additive white Gaussian noise (AWGN) channel [8]. In each of these four methods, the electrical power dissipation penalty relative to a bipolar OFDM signal is only 3 dB for any $M$-QAM constellation size. This introduces a significant energy advantage over DCO-OFDM. Note also that the concepts of Flip-OFDM and U-OFDM are equivalent, and both terms exist in the literature as the two schemes have been developed and published independently [11], [12].

The signal generation process for ACO-OFDM, PAM-DMT, Flip-OFDM, and U-OFDM sacrifices half of the spectral efficiency compared to a DCO-OFDM signal with the same $M$-QAM constellation size. This means that $M$-QAM DCO-OFDM should be compared to $M^2$-QAM ACO-OFDM/U-OFDM/Flip-OFDM and to $M$-PAM PAM-DMT in order to keep the achievable data rate equivalent. As a consequence, all four inherently unipolar modulation schemes incur a substantial loss of energy efficiency compared to DCO-OFDM for a spectral efficiency above 1 bit/s/Hz [13]. Dissanayake *et al.* [14] have proposed a technique to simultaneously transmit ACO-OFDM and DCO-OFDM in an attempt to close the spectral efficiency gap. However, this method still requires a DC-bias for the generation of DCO-OFDM. Asadzadeh *et al.* [15] have proposed an alternative modulation method named spectrally factorized optical OFDM (SFO-OFDM). It analyses the frequency-domain signal requirements that lead to an inherently unipolar OFDM signal and attempts to generate a modified set of constellation symbols which can always fulfil these requirements. However, this concept appears to be infeasible for practical implementation due to its complexity.

The current work introduces an algorithm, named eU-OFDM, to simultaneously transmit multiple unipolar data streams which do not require any added bias. As a result, the spectral efficiency loss of U-OFDM is compensated while a significant energy advantage over DCO-OFDM is retained. In this paper, the feasibility of U-OFDM and of eU-OFDM is demonstrated for the first time in a proof-of-concept experimental set-up of a VLC link.

The rest of this paper is organized as follows. Section II provides an overview of U-OFDM. Section III introduces the modified modulation approach. Section IV makes a performance comparison between the proposed novel method and DCO-OFDM. Section V presents an experimental study where the merits of eU-OFDM are investigated in practice. Finally, Section VI provides concluding remarks.

## II. U-OFDM

In U-OFDM [11], the real bipolar signal produced by the IFFT operation in the OFDM modulation process is transformed into a unipolar signal by a simple transformation in the time domain. Two copies of each bipolar frame are placed one after the other in the modulation signal. The second copy is multiplied by $-1$. Afterwards, all negative samples from both copies are set to zero. Therefore, the first instance of the original bipolar frame holds the positive time-domain samples and zeros in place of the negative ones. In the context of this work, this frame instance will be referred to as the *positive* frame. The second instance of the original bipolar frame holds the absolute values of the negative samples and zeros in place of the positive ones. This frame instance will be referred to as the *negative* frame. The signal generation procedure is illustrated in Fig. 1(a) and (b). The time-domain signal transformation halves the achievable data rate and effectively halves the spectral efficiency which becomes:

$$\eta_{\mathrm{U}} = \frac{\sum\limits_{\substack{k=1 \\ M_k>0}}^{\frac{N_{\mathrm{fft}}}{2}-1} \log_2(M_k)}{2(N_{\mathrm{FFT}}+N_{\mathrm{cp}})} \text{ bits/s/Hz}, \tag{1}$$

as opposed to the spectral efficiency of DCO-OFDM:

$$\eta_{\mathrm{DCO}} = \frac{\sum\limits_{\substack{k=1 \\ M_k>0}}^{\frac{N_{\mathrm{fft}}}{2}-1} \log_2(M_k)}{(N_{\mathrm{FFT}}+N_{\mathrm{cp}})} \text{ bits/s/Hz}. \tag{2}$$

The factor $\log_2(M_k)$ indicates the number of bits that are encoded in the $M$-QAM constellation at subcarrier $k$; $N_{\mathrm{FFT}}$ is the FFT size; the factor 1/2 appears in (1) because U-OFDM transmits two frame instances for every bipolar frame; and $N_{\mathrm{cp}}$ is the length of the cyclic prefix.

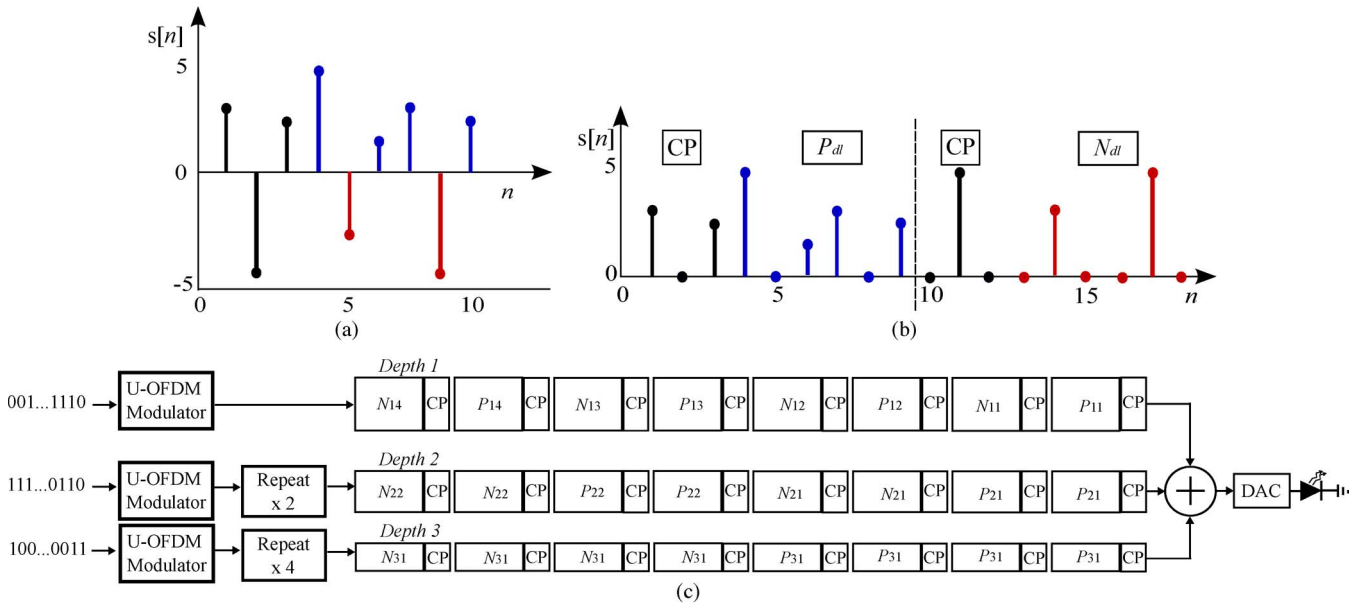


Fig. 1. Enhanced U-OFDM for a maximum modulation depth of 3. CP denotes the OFDM cyclic prefix in every frame. $P_{dl}$ is the $l$th *positive* frame at *Depth d*. $N_{dl}$ is the $l$th *negative* frame at *Depth d*. The presented digital-to-analog converter (DAC) block includes all processing techniques and electrical circuitry required for transition from a discrete-time-domain signal to a continuous analog signal capable of modulating the LED transmitter. (a) Bipolar OFDM. (b) Unipolar OFDM. (c) Enhanced Unipolar OFDM.

At the U-OFDM receiver, each original bipolar frame is recovered by subtracting the samples in the *negative* frame from the samples in the *positive* frame. The subtraction operation combines the AWGN at the *positive* and the *negative* frame which causes the signal-to-noise ratio (SNR) to drop by 3 dB compared to the achievable SNR at the receiver when a bipolar real OFDM signal is transmitted. As described in Section I, a bipolar signal cannot be used in an IM/DD system. However, in this work, the performance of a bipolar real signal is referred to for comparison purposes. As already noted in Section I, the DC-bias in DCO-OFDM causes a substantial increase in the energy consumption. The bias level is defined as:

$$b_{\mathrm{DC}} = k_{\mathrm{DC}}\sqrt{\mathrm{E}\left\{\mathrm{s}^2(t)\right\}} = k_{\mathrm{DC}}\sigma_{\mathrm{s}}, \tag{3}$$

where $\mathrm{s}(t)$ denotes the time-domain bipolar OFDM signal, and $\mathrm{E}\{\cdot\}$ denotes statistical expectation. Then, compared to a bipolar OFDM signal, the electrical energy dissipation of DCO-OFDM increases by [16]:

$$10\log_{10}\left(k_{\mathrm{DC}}^2 + 1\right)\ \mathrm{dB}. \tag{4}$$

This statement is true only if the biasing level is sufficiently high such that clipping of any values which are still negative after the biasing operation does not affect the performance and the energy dissipation significantly [16]. For practical calculations, this assumption can be made. Monte Carlo simulations have shown, for example, that the minimum biasing requirement of 4-QAM DCO-OFDM leads to an electrical power penalty of approximately 6–7 dB when compared to a bipolar OFDM signal for a bit error rate (BER) of approximately $10^{-3}$ to $10^{-4}$. If the modulation order is increased, this penalty increases as well. Hence, U-OFDM is clearly more power efficient than DCO-OFDM for the same constellation size. However, as noted in Section I, the halving of the spectral efficiency in U-OFDM means that $M$-QAM DCO-OFDM should be compared to $M^2$-QAM U-OFDM for a fair performance estimation. Consequently, as $M$ is increased, U-OFDM very quickly loses its energy efficiency over DCO-OFDM.

In [11], an improved decoder is presented for U-OFDM. The improved decoding algorithm applies a modified recombination technique for the *positive* and *negative* frames. Instead of using subtraction, the improved technique attempts to guess whether the *positive* or the *negative* frame contains the value of the original bipolar sample at each position of the OFDM frame. The decoding algorithm simply selects the sample with the higher amplitude between the two frames and discards the sample in the other frame. Ideally, this technique can remove half of the AWGN energy and can make the performance of U-OFDM equivalent to the performance of a bipolar OFDM signal for the same $M$-QAM constellation size. However, it cannot compensate for the power penalty that results from the requirement for a higher constellation size in comparison to DCO-OFDM. Furthermore, this technique can only be applied in a relatively flat communication channel where ISI is not significant. If the ISI is not negligible, then this demodulation technique requires equalisation to be performed in the time domain before any sample selection. In addition, because this method discards half of the U-OFDM time-domain samples, the communication channel cannot really be analysed in the frequency domain. This renders the use of adaptive bit and energy loading techniques difficult. Furthermore, it should be noted that frequency-dependent distortion effects caused, for example, by the DC-wander effect in electrical circuits as well as by flickering noise from ambient light sources could become unavoidable and could further hinder the performance of this demodulation algorithm.

## III. Enhanced U-OFDM

The current work presents a modified version of U-OFDM which can effectively compensate the spectral efficiency loss described in Section II. The concept is illustrated in Fig. 1(c). It allows multiple U-OFDM streams to be combined in a single time-domain signal that can be used to modulate the LED.

### A. Modulation Concept

The information stream that is depicted at *Depth 1* in Fig. 1(c) represents a conventional U-OFDM time-domain signal. The *positive* frames are labelled with *P* and the *negative* frames are labelled with *N*. The signal at *Depth 1* is generated as described in Section II. A second U-OFDM information stream, presented at *Depth 2* in Fig. 1(c), can be superimposed on the first one. The additional stream does not affect the ability of the receiver to recover the transmitted bits as long as any signal components of the second stream that fall within the duration of a given *positive* frame from the first stream are equivalent to the signal components of the second stream that fall within the duration of the subsequent *negative* frame from the first stream. This occurs because the subtraction operation in the demodulation procedure cancels out any equivalent interference components. Therefore, at *Depth 2*, each U-OFDM frame is transmitted twice in a row. Hence, in Fig. 1(c), the second frame at *Depth 2* is an exact copy of the first frame, the fourth frame is an exact copy of the third frame, etc., as indicated by the respective labels. Because each U-OFDM frame is transmitted twice at *Depth 2*, the amplitude of each frame instance is scaled by $\sqrt{1/2}$ in order to keep the energy per bit at each depth constant. A third stream can be added analogously to the second stream. At *Depth 3*, the U-OFDM frames have to be replicated four times in order to keep the interference over the first two streams in the desired format. The amplitude of each frame instance at *Depth 3* is scaled by $\sqrt{1/4}$ in order to keep the energy per bit at all streams constant. Additional information streams could be added analogously where each U-OFDM frame is replicated into $2^{d-1}$ consecutive frames whose amplitude is scaled by $1/\sqrt{2^{d-1}}$, where $d$ indicates the stream depth.

At the receiver site, the information at *Depth 1* can be recovered using the conventional technique for U-OFDM as described in Section II. First, each *negative* frame is subtracted from each *positive* frame. Then the conventional OFDM demodulation techniques are applied on the obtained bipolar frames. For the example in Fig. 1(c), at *Depth 1*, the first bipolar frame is recovered with the operation $P_{11} - N_{11}$. The second bipolar frame is recovered with the operation $P_{12} - N_{12}$, etc. The additional streams do not hinder the demodulation process because the interference that falls on $P_{11}$ is equivalent to the interference that falls on $N_{11}$ caused by $P_{21} + P_{31}$. Hence, the subtraction operation completely removes the interference terms. The same interference cancellation occurs for all subsequent frames at *Depth 1*. As a result, the information at *Depth 1* is completely recovered with the conventional U-OFDM demodulator. After the information bits at *Depth 1* are obtained, they are remodulated again and the original U-OFDM signal at *Depth 1* is regenerated. This signal is then subtracted from the overall received signal. The result contains only the information streams at *Depth 2* and subsequent depths. At *Depth 2*, every two equivalent frames are summed. For example, the first frame and the second frame at *Depth 2* are summed, the third frame and the fourth frame are summed, etc.. Afterwards, the demodulation process continues with conventional U-OFDM demodulation just as in the case at *Depth 1*. At all depths, interference from subsequent streams does not affect the information recovery process due to the employed signal structure. After the information bits are recovered at each depth, they are remodulated and the result is subtracted from the remaining received signal. This iterative demodulation procedure is applied until the binary data at all depths is decoded.

TABLE I
Spectral Efficiency of eU-OFDM

| $D$ | 1 | 2 | 3 | 4 | 5 | 6 | 7 |
|---|---|---|---|---|---|---|---|
| $\frac{\eta_{\mathrm{eU}}(D)}{\eta_{\mathrm{DCO}}}$ [%] | 50 | 75 | 87.5 | 93.75 | 96.88 | 98.44 | 99.22 |

### B. Spectral Efficiency

The enhanced U-OFDM scheme has higher spectral efficiency than U-OFDM. It can be calculated as the sum of the information streams' spectral efficiencies at all depths:

$$\eta_{\mathrm{eU}}(D) = \sum_{d=1}^{D} \frac{\eta_{\mathrm{U}}}{2^{d-1}} = \eta_{\mathrm{U}} \sum_{d=1}^{D} \frac{1}{2^{d-1}}, \tag{5}$$

where $D$ is the maximum modulation depth of the scheme, which equals the total number of U-OFDM streams that are superimposed in the modulation signal. The spectral efficiency of eU-OFDM increases with the increase of the maximum modulation depth as illustrated in Table I. For a large modulation depth, $\eta_{\mathrm{eU}}(D)$ converges to the spectral efficiency of DCO-OFDM:

$$\lim_{D\to\infty} \eta_{\mathrm{eU}}(D) = \eta_{\mathrm{U}} \lim_{D\to\infty} \sum_{d=1}^{D} \frac{1}{2^{d-1}} = 2\eta_{\mathrm{U}} = \eta_{\mathrm{DCO}}. \tag{6}$$

Two practical implementation issues need to be considered. Firstly, transmission in OFDM cannot start before at least a full block of bits, required for the generation of one full OFDM frame, is available at the transmitter. This introduces a latency of at least one frame length in real-time streaming applications. In eU-OFDM, this latency increases with the modulation depth since the binary data for at least $2^D - 1$ OFDM frames has to be available at the transmitter before one full eU-OFDM data block, as depicted in Fig. 1(c), can be generated and the transmission can begin. Some latency is expected at the receiver since at least $2^d$ frames need to be received before the demodulation at depth $d$ can be completed successfully. Secondly, it can be assumed that the computational complexity in OFDM is dominated by the FFT/IFFT operation [12]. The demodulation process in eU-OFDM requires additional FFT/IFFT operations to be performed at the receiver. If all subtraction procedures are performed in the time domain, then the number of FFT/IFFT operations would be approximately

double the number of FFT/IFFT operations required in conventional OFDM since each demodulated frame has to be remodulated and, therefore, requires an additional IFFT operation. In a communication channel with a non-flat frequency profile this would introduce additional equalization complexity as the remodulated signal components would also need to be distorted by the channel transfer characteristic before they are subtracted from the received signal. Hence, it might be more practical if all subtraction operations are performed in the frequency domain after the FFT operation. Then, equalization needs to be performed only once per frame interval. In this implementation, however, the number of required FFT/IFFT operations is approximately four times that in conventional OFDM demodulation. The implementation of eU-OFDM also comes with an increase in the required memory because the data equivalent of $2^D$ OFDM frames has to be buffered for the demodulation of one full eU-OFDM block such as the one depicted in Fig. 1(c).

The implementation issues put a practical limit on the maximum eU-OFDM modulation depth that can be realized for a given hardware cost budget. We believe that in practical applications, the hardware complexity is not going to be problematic since for a relatively small maximum modulation depth, the gap in spectral efficiency between eU-OFDM and DCO-OFDM is practically closed. For example, for a maximum modulation depth between $D = 3$ and $D = 5$, $\eta_{\mathrm{eU}}$ is already between 87.5% and 96.88% of $\eta_{\mathrm{DCO}}$, which means the difference is negligible. A detailed analysis of the implementation cost of eU-OFDM is outside the scope of this paper and will be addressed in future work.

### C. Power Efficiency

*1) Electrical Power:* The bipolar OFDM signal follows a Gaussian distribution in the time domain with average electrical power of $\mathrm{E}\{\mathrm{s}^2(t)\}=\sigma_s^2$, where $\sigma_\mathrm{s}$ is the standard deviation of the time-domain waveform $\mathrm{s}(t)$ [8], [17]. Half of the time-domain samples of a U-OFDM signal follow a truncated Gaussian distribution and the other half are equal to zero [8], [11]. Hence, it is straightforward to derive that the average power of the U-OFDM waveform is $\sigma_\mathrm{s}^2/2$ [8], [11]. The eU-OFDM signal is a combination of independent U-OFDM streams, and, therefore, its average electrical power is expected to be higher. It can be calculated as [8], [16]:

$$\begin{aligned} P_{\mathrm{elec,eU}}^{\mathrm{avg}} &= \mathrm{E}\left\{\mathrm{s}_{\mathrm{eU}}^2(t)\right\} = \mathrm{E}\left\{\left(\sum_{d=1}^{D}\underline{\mathrm{s}}_d(t)\right)^2\right\} \\ &= \sum_{d=1}^{D}\mathrm{E}\left\{\underline{\mathrm{s}}_d^2(t)\right\} + \sum_{d_1=1}^{D}\sum_{\substack{d_2=1\\ d_1\neq d_2}}^{D}\mathrm{E}\left\{\underline{\mathrm{s}}_{d_1}(t)\right\}\mathrm{E}\left\{\underline{\mathrm{s}}_{d_2}(t)\right\} \\ &= \frac{\sigma_\mathrm{s}^2}{2}\sum_{d=1}^{D}\frac{1}{2^{d-1}} + \sum_{d_1=1}^{D}\sum_{\substack{d_2=1\\ d_1\neq d_2}}^{D}\frac{\phi(0)\sigma_\mathrm{s}}{\sqrt{2^{d_1-1}}}\frac{\phi(0)\sigma_\mathrm{s}}{\sqrt{2^{d_2-1}}} \\ &= \frac{\sigma_\mathrm{s}^2}{2}\left(2-\frac{1}{2^{D-1}}\right)+\frac{\sigma_\mathrm{s}^2}{2}4\phi^2(0)\sum_{d_1=1}^{D}\sum_{\substack{d_2=1\\ d_1\neq d_2}}^{D}\frac{1}{\sqrt{2^{d_1+d_2}}}, \end{aligned} \tag{7}$$

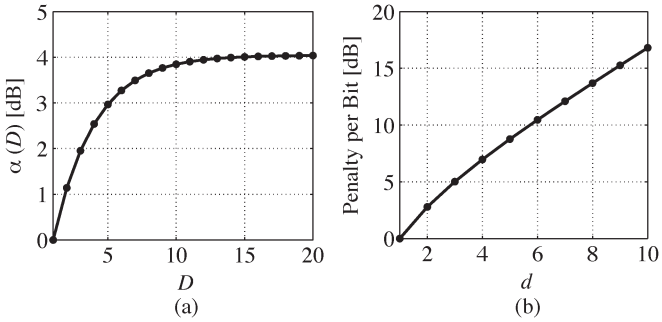


Fig. 2. Energy penalty with increasing modulation depth: (a) average penalty per bit as a function of the maximum modulation depth; (b) Penalty per additional bit at a specific depth.

TABLE II
ENERGY PENALTY FOR EU-OFDM RELATIVE TO U-OFDM

| $D$ | 1 | 2 | 3 | 4 | 5 | 6 | 7 |
|---|---|---|---|---|---|---|---|
| $\alpha(D)$ [dB] | 0 | 1.14 | 1.95 | 2.54 | 2.97 | 3.27 | 3.49 |

where $\mathrm{s}_{\mathrm{eU}}(t)$ is the time-domain eU-OFDM waveform; $\underline{\mathrm{s}}_d(t)$ is the time-domain U-OFDM signal at depth $d$; and $\phi(0)$ is the probability density function (PDF) of the standard normal distribution. The time-domain expectation of the U-OFDM signal at depth $d$, $\mathrm{E}\{\underline{\mathrm{s}}_d(t)\}=\phi(0)\sigma_\mathrm{s}/\sqrt{2^{d-1}}$, used in (7), is derived from the statistics of the truncated Gaussian distribution described in more detail in [18]. The number of bits conveyed in eU-OFDM is $2-1/2^{D-1}$ times more than the number of bits conveyed in U-OFDM for the same time interval. Therefore, the increase in the required SNR per bit compared to U-OFDM for the same $M$-QAM constellation size is:

$$\alpha(D) = 1 + \frac{4\phi^2(0)}{2-1/2^{D-1}}\sum_{d_1=1}^{D}\sum_{\substack{d_2=1\\ d_1\neq d_2}}^{D}\frac{1}{\sqrt{2^{d_1+d_2}}}. \tag{8}$$

The electrical SNR of the system is defined as [8], [16]:

$$\frac{E_{\mathrm{b,elec}}}{N_\mathrm{o}} = \frac{P_{\mathrm{elec,eU}}^{\mathrm{avg}}}{2B\eta_{\mathrm{eU}}N_\mathrm{o}} = \frac{\mathrm{E}\left\{\mathrm{s}_{\mathrm{eU}}^2(t)\right\}}{2B\eta_{\mathrm{eU}}N_\mathrm{o}}, \tag{9}$$

where $B$ is the employed single-sided communication bandwidth and $N_\mathrm{o}$ is the single-sided power spectral density (PSD) of the AWGN at the receiver. Note that in the literature the convention of whether $N_\mathrm{o}$ refers to the double-sided or the single-sided PSD of the noise component may differ leading to a 3 dB shift in all presented results. Fig. 2(a) shows $\alpha(D)$ for different values of the maximum modulation depth. In addition, Table II presents $\alpha(D)$ for a maximum modulation depth of up to $D = 7$. The average SNR penalty of eU-OFDM in comparison to U-OFDM converges to about 4 dB as the spectral efficiency converges to the spectral efficiency of DCO-OFDM. As described in Section II, U-OFDM has a constant SNR penalty of 3 dB when compared to a bipolar OFDM signal. Therefore, irrespective of the employed $M$-QAM constellation size, eU-OFDM can incur a maximum electrical SNR penalty

of about 7 dB when compared to a bipolar OFDM signal. As described in Section II, in DCO-OFDM, the electrical SNR penalty relative to a bipolar OFDM signal begins at around 6–7 dB for 4-QAM and increases with the modulation order because larger constellations are more sensitive to non-linear distortion, and, therefore, require higher biasing levels in order to reduce the clipping effect on any negative signal samples. Consequently, depending on the employed $M$-QAM constellation size, eU-OFDM is expected to have comparable or better performance than DCO-OFDM.

The additional energy per bit that is introduced at each modulation depth, $d$, is shown in Fig. 2(b). The curve shows the extra energy per extra bit that is added at each modulation depth. Since additional streams are added on top of an already existing time-domain signal, the energy per additional bit that they introduce increases significantly with the modulation depth. This means that adding additional streams to close the spectral efficiency gap between eU-OFDM and DCO-OFDM quickly becomes energy inefficient. When latency, hardware complexity and the spectral efficiency gap, illustrated in Table I, are also taken into account, it can be seen that a practical implementation is likely to be realized for a maximum modulation depth of only a few streams. In case the spectral efficiency gap has to be closed completely, an alternative eU-OFDM implementation with different $M$-QAM constellation sizes at each depth can be considered. For example, two 16-QAM streams are enough to match the spectral efficiency of 8-QAM DCO-OFDM; and a 64-QAM stream followed by a 16-QAM stream or a combination of a 32-QAM stream and two subsequent 16-QAM streams is enough to match the spectral efficiency of 16-QAM DCO-OFDM. A detailed study of optimal stream combinations is outside the scope of this work but will be conducted in future work.

A theoretical bound on the BER performance of eU-OFDM as a function of the SNR can be estimated by using the formula for calculating the BER of conventional real bipolar $M$-QAM OFDM. The only modification required in that formula is to scale the required SNR at the receiver by a factor of $2\alpha(D)$ to account for the U-OFDM performance degradation and to account for the SNR penalty in eU-OFDM. Hence, using the BER formula for $M$-QAM in [19], the BER for eU-OFDM can be expressed as:

$$\begin{aligned}&\mathrm{BER}_{\mathrm{eU}}\left(M, \frac{E_{\mathrm{b,elec}}}{N_{\mathrm{o}}}\right)\\ &= \mathrm{BER}_{\mathrm{QAM}}\left(M, \frac{1}{2\alpha(D)}\frac{E_{\mathrm{b,elec}}}{N_{\mathrm{o}}}\right)\\ &= \frac{4}{\log_2 M}\left(1-\frac{1}{\sqrt{M}}\right)\\ &\quad\times \sum_{l=1}^{\min(2,\sqrt{M})} \mathrm{Q}\left((2l-1)\sqrt{\frac{3E_{\mathrm{b,elec}}\log_2 M}{2\alpha(D)(M-1)N_{\mathrm{o}}}}\right).\end{aligned} \tag{10}$$

The proposed bound coincides with the BER curve for the information stream at *Depth 1* in eU-OFDM where distortion is caused only by the AWGN at the receiver as the inter-stream interference is completely removed by the subtraction operation in the demodulation algorithm. The BER of the subsequent streams increases with the depth because the performance of every stream is affected by the BER of the previous streams. Any incorrectly demodulated bits at a given depth translate into imperfections in the iterative stream cancellation algorithm, which results in reduced signal quality at all subsequent depths. As the SNR increases and the bit errors are reduced, the performance of all streams converges to the performance of the stream at *Depth 1*. This trend is shown in Fig. 3. The presented results also show a very good match between the theoretical performance bound and the results of Monte Carlo simulations.

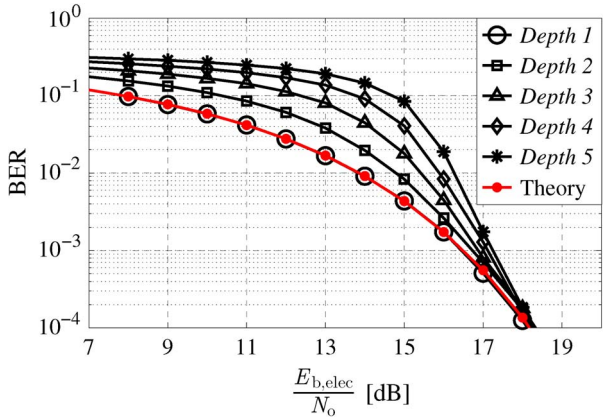


Fig. 3. 16-QAM eU-OFDM performance at different depths as a function of the electrical SNR. The curve "Theory" represents the theoretically-derived performance bound.

*2) Optical Power:* The average optical power of the eU-OFDM signal is calculated as [8], [16]:

$$\begin{aligned}P_{\mathrm{opt,eU}}^{\mathrm{avg}} &= \mathrm{E}\left\{\mathrm{s}_{\mathrm{eU}}(t)\right\} = \mathrm{E}\left\{\sum_{d=1}^{D}\underline{\mathrm{s}}_d(t)\right\} = \sum_{d=1}^{D}\mathrm{E}\left\{\underline{\mathrm{s}}_d(t)\right\}\\ &= \phi(0)\sigma_{\mathrm{s}}\sum_{d=1}^{D}\frac{1}{\sqrt{2^{d-1}}}.\end{aligned} \tag{11}$$

where the optical SNR of the system is defined as [8], [16]:

$$\frac{E_{\mathrm{b,opt}}}{N_{\mathrm{o}}} = \frac{P_{\mathrm{opt,eU}}^{\mathrm{avg}}}{2B\eta_{\mathrm{eU}}N_{\mathrm{o}}} = \frac{\mathrm{E}\left\{\mathrm{s}_{\mathrm{eU}}(t)\right\}}{2B\eta_{\mathrm{eU}}N_{\mathrm{o}}}. \tag{12}$$

The relationship between the electrical SNR and the optical SNR can be expressed as the ratio of (7) and (11):

$$\alpha_{\mathrm{o-e}}(D) = \frac{P_{\mathrm{elec,eU}}^{\mathrm{avg}}}{P_{\mathrm{opt,eU}}^{\mathrm{avg}}}. \tag{13}$$

Therefore, for any value of the optical SNR, the equivalent electrical SNR can be derived according to this relationship. Then, the already derived closed-form BER bound as a function of the electrical SNR can be used to calculate a performance bound as a function of the optical SNR:

$$\mathrm{BER}_{\mathrm{eU}}\left(M, \frac{E_{\mathrm{b,opt}}}{N_{\mathrm{o}}}\right) = \mathrm{BER}_{\mathrm{QAM}}\left(M, \frac{\alpha_{\mathrm{o-e}}(D)}{2\alpha(D)}\frac{E_{\mathrm{b,opt}}}{N_{\mathrm{o}}}\right). \tag{14}$$

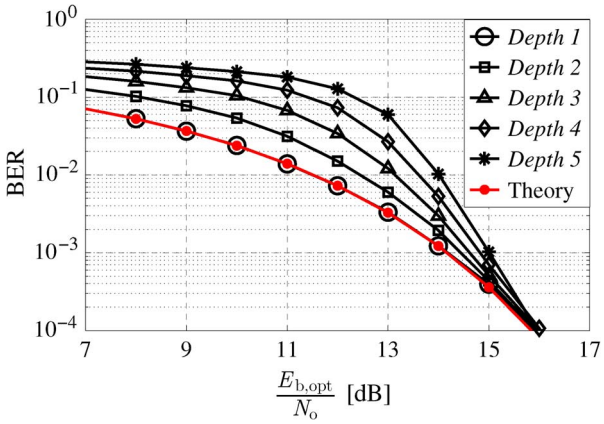


Fig. 4. 16-QAM eU-OFDM performance at different depths as a function of the optical SNR. The curve "Theory" represents the theoretically-derived performance bound.

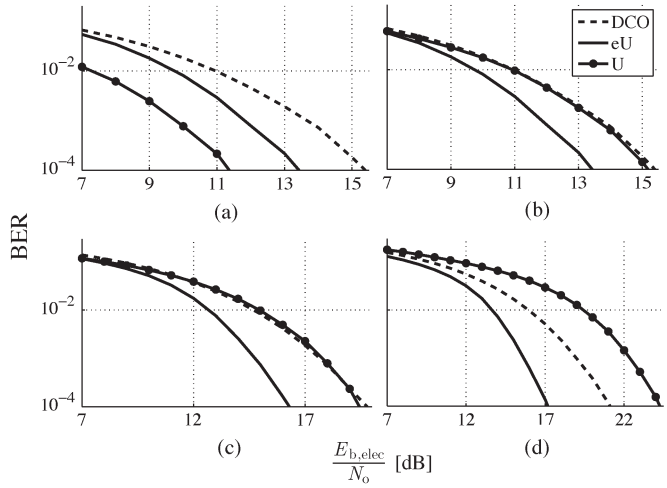


Fig. 5. Performance comparison between eU-OFDM, U-OFDM, and DCO-OFDM for different $M$-QAM constellation sizes as a function of the electrical SNR: (a) BPSK; (b) 4-QAM; (c) 8-QAM; (d) 16-QAM. Optimum biasing levels for BPSK, 4-QAM, 8-QAM, and 16-QAM DCO-OFDM are estimated through Monte Carlo simulations at respectively 6 dB, 6 dB, 7 dB, and 7.5 dB, as described in (4).

Fig. 4 shows very close agreement between the proposed theoretical analysis and the Monte Carlo simulations conducted. All calculations presented so far are made for an ideal front-end device under the assumption that eU-OFDM modulation does not require biasing of the LED. However, an LED typically requires a minimum bias voltage at which the device begins to conduct electricity and emit light. A zero bias can be assumed for the estimation of the optical efficiency of the system because at the lowest operational point of the LED, the light intensity output can be assumed negligible. However, for the calculation of the electrical efficiency, the bias generally has to be taken into account. As long as it is small, relative to the dynamic range of the information signal, the bias would not introduce significant variations from the estimated energy efficiency of the system. Furthermore, this minimum required biasing value is device-specific. Therefore, in the current theoretical study, it is neglected in order to simplify the analysis. The experimental results, presented in Section V, take this biasing into account.

## IV. Simulation Results

This section investigates the performance of eU-OFDM in the context of a linear AWGN channel. The only non-linear effect included in this study is clipping of any negative values in the modulation signal due to the electrical characteristics of an ideal LED. In practical scenarios, an information signal can also be clipped from above due to saturation of the optical output intensity and due to maximum current and optical radiation constraints. These effects are device-specific and are strongly dependent on the particular practical scenario. Hence, they are not considered in this study. Clipping of the modulation signal from below, however, is relevant to all devices. It cannot be avoided in a scheme such as DCO-OFDM due to the high peak-to-average power ratio (PAPR) of an OFDM signal which increases linearly with the number of active subcarriers in the frequency domain [20], [21]. The newly-introduced modulation scheme, eU-OFDM, is strictly positive and so it completely avoids clipping of the signal from below. In the current study, the maximum modulation depth of eU-OFDM is set to $D = 3$ because this value closes most of the spectral efficiency gap between DCO-OFDM and U-OFDM. In addition, a smaller maximum modulation depth simplifies the implementation described in Section V. Therefore, in all of the presented results for the rest of this section, the spectral efficiency of eU-OFDM is actually 87.5% of the spectral efficiency of DCO-OFDM as shown in Table I. At the same time, in each of the cases where the performance of U-OFDM is also presented, the constellation size in U-OFDM is selected such that the spectral efficiency of U-OFDM (expressed in (1)) matches exactly the spectral efficiency of DCO-OFDM (expressed in (2)).

The average BER of the information at all depths in eU-OFDM is compared with the BER of DCO-OFDM and U-OFDM for different $M$-QAM constellation sizes. Fig. 5 presents the results as a function of the electrical SNR for constellation sizes of $M = [2, 4, 8, 16]$. In U-OFDM, an actual constellation size of $M^2$ is employed for each respective value of $M$ in order to ensure equal spectral efficiency between the three schemes. Results have been presented for BER values down to $10^{-4}$ as most forward error correction (FEC) codes would be able to deliver reliable communication for such BER values [22]. The performance improvement of eU-OFDM over DCO-OFDM starts at around 2 dB for binary phase-shift keying (BPSK) and increases to about 4 dB for 16-QAM. The DCO-OFDM bias levels for the different $M$-QAM constellations have been optimised through Monte Carlo simulations, in agreement with previous work as in [18], [23]. This means that adding less bias would lead to more clipping and, hence, to higher non-linear distortion and higher BER for a given SNR. Adding more bias would lead to higher energy dissipation without actually reducing the BER. In each of the presented cases, the bias level is expressed as the estimated SNR increase in dB compared to a bipolar OFDM signal, as described in (4). Note that, for a maximum depth of $D = 3$, the SNR penalty in eU-OFDM is $\alpha \approx 1.95$ dB as shown in Fig. 2(a). The SNR penalty is constant

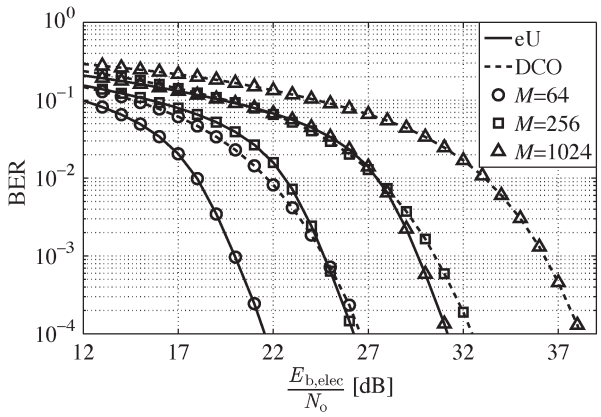


Fig. 6. eU-OFDM performance vs. DCO-OFDM performance for different $M$-QAM constellation sizes as a function of the electrical SNR. Optimum biasing levels for 64-QAM, 256-QAM, and 1024-QAM DCO-OFDM are estimated at respectively 9.5 dB, 11 dB, and 13 dB, as described in (4).

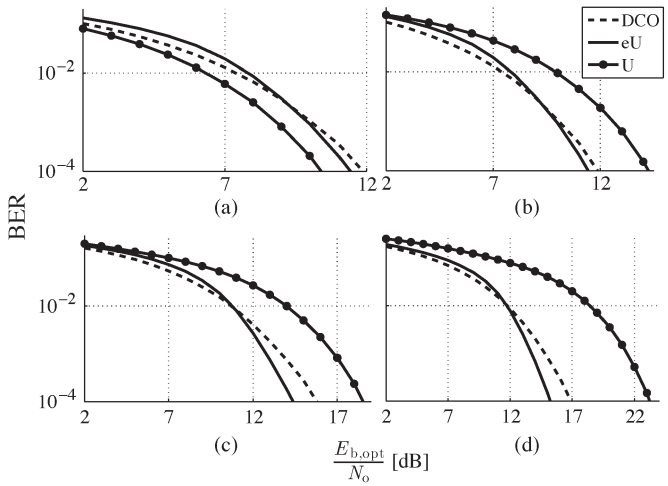


Fig. 7. Performance comparison between eU-OFDM, U-OFDM, and DCO-OFDM for different $M$-QAM constellation sizes as a function of the optical SNR: (a) BPSK; (b) 4-QAM; (c) 8-QAM; (d) 16-QAM. Optimum biasing levels for BPSK, 4-QAM, 8-QAM, and 16-QAM DCO-OFDM are estimated through Monte Carlo simulations at respectively 6 dB, 6 dB, 7 dB, and 7.5 dB, as described in (4).

for all constellation sizes. This explains and quantifies the increase in energy efficiency of eU-OFDM over DCO-OFDM with an increase in the $M$-QAM modulation order. Fig. 5 also illustrates the loss in energy efficiency of U-OFDM as the spectral efficiency increases. In Fig. 5(a), 4-QAM U-OFDM is more energy efficient than both BPSK eU-OFDM and BPSK DCO-OFDM. In Fig. 5(b) and (c), 16-QAM U-OFDM and 64-QAM U-OFDM are already less energy efficient than 4-QAM eU-OFDM and 8-QAM eU-OFDM, respectively, while at the same time exhibiting approximately the same performance as 4-QAM DCO-OFDM and 8-QAM DCO-OFDM. In Fig. 5(d), 256-QAM U-OFDM is less energy efficient than both 16-QAM eU-OFDM and 16-QAM DCO-OFDM. Fig. 7 illustrates the same performance trends for all three investigated schemes as a function of the optical SNR. For BPSK and 4-QAM, eU-OFDM has an efficiency advantage of about 0.5 dB over DCO-OFDM. This advantage reaches almost 2 dB for 16-QAM. At the same time, U-OFDM shows advantage only for a constellation size of $M = 4$ against BPSK eU-OFDM/DCO-OFDM in Fig. 7(a).

A performance comparison between eU-OFDM and DCO-OFDM has also been conducted for higher spectral efficiencies. Results for $M = [64, 256, 1024]$ are presented in Fig. 6 and Fig. 8. U-OFDM is not included in this study as it was already shown that it loses its energy advantage over both eU-OFDM and DCO-OFDM for 256-QAM U-OFDM versus 16-QAM eU-OFDM/DCO-OFDM. The results presented in Fig. 6 and Fig. 8 indicate that for 1024-QAM, eU-OFDM could attain savings of around 7 dB in electrical energy dissipation over DCO-OFDM, and savings of around 3 dB in required optical power, which could make a significant difference in future high-speed OWC systems.

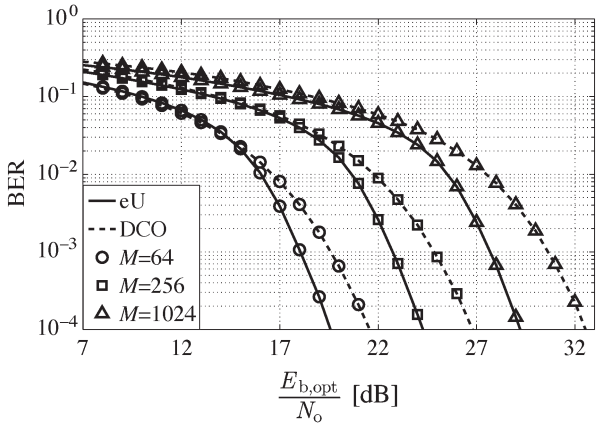


Fig. 8. eU-OFDM performance vs. DCO-OFDM performance for different $M$-QAM constellation sizes as a function of the optical SNR. Optimum biasing levels for 64-QAM, 256-QAM, and 1024-QAM DCO-OFDM are estimated at respectively 9.5 dB, 11 dB, and 13 dB, as described in (4).

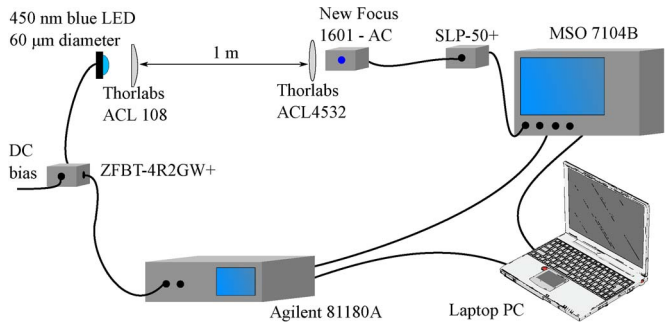


Fig. 9. Experimental set-up.

## V. Experimental Results

An experimental system was set up in order to realize a proof-of-concept implementation for U-OFDM and eU-OFDM and also to compare their performance against the performance of DCO-OFDM. The experimental set-up is illustrated in Fig. 9. It closely resembles the set-up described in [6], where, to the best of the authors' knowledge, the fastest single-LED wireless link was recently demonstrated using a GaN micro light emitting diode ($\mu$LED).

### A. Experimental Setup

A discrete OFDM/U-OFDM/eU-OFDM signal is generated in MATLAB® through a series of steps that include: random bit generation, $M$-QAM modulation, IFFT, oversampling, and pulse shaping. In U-OFDM and eU-OFDM, the pulse shaping is performed after the *positive* and the *negative* frame are generated, as described in Section II, but before any negative values are removed. This is consistent with the work presented in [24]. The discrete time samples of the OFDM/U-OFDM/eU-OFDM signal are passed to an arbitrary waveform generator (AWG), Agilent 81180A, which performs digital-to-analog conversion with a 12-bit zero-order-hold digital-to-analog converter (DAC), and outputs an analog waveform used to modulate the LED. The AWG has a DC-coupled output amplifier with a maximum voltage swing of 2 V and a maximum output DC offset of 1.5 V. The LED has a turn-on voltage of almost 3 V. Therefore, in order to fit the information signal within the active range of the LED, additional bias is added to the information signal via a bias-T, Mini Circuits ZFBT-4R2GW+. The output of the bias-T directly modulates the voltage over the LED. The light emitted from the LED is collimated via an aspheric lens, Thorlabs ACL108, and directed towards the receiver. At the receiver site, an aspheric lens, Thorlabs ACL4532, collects the received light and focuses it on a positive-intrinsic-negative (PIN) photodetector, New Focus 1601-AC. The photodetector outputs a continuous analog signal which is filtered with a 48 MHz passive low-pass filter, Mini Circuits SLP-50+, and sampled by a digital oscilloscope, Agilent MSO7104B. The latter device performs digital to analog conversion with a 12-bit analog-to-digital converter (ADC). The bandwidth of the oscilloscope channel is limited to 25 MHz in order to remove excess AWGN from the receiver, which has a bandwidth of 1 GHz. The digitized signal is retrieved from the oscilloscope and processed in MATLAB® through a series of steps that include: synchronization, matched filtering, downsampling, FFT, channel estimation, equalization, and $M$-QAM demodulation. Any additional demodulation steps relevant to U-OFDM and eU-OFDM are performed according to the description provided in Sections II and III.

The relevant OFDM parameters are: 1) an FFT size $N_{\text{fft}} = 1024$, of which only 511 subcarriers can be modulated with unique information due to the requirement to impose Hermitian symmetry in the frequency domain in order to generate a real time-domain OFDM signal [8], [23]; 2) cyclic prefix length of $N_{\text{cp}} = 5$; 3) single-sided communication bandwidth of $B = 20$ MHz over which the frequency response of the LED is flat according to [6]; the single-sided bandwidth of the eU-OFDM signal is set to 23 MHz in all of the conducted experiments in order to compensate for the spectral efficiency difference of 12.5% between eU-OFDM and the other two schemes; thus, the achievable data rate in all three systems is equivalent; 4) digital clipping of the OFDM signal at $-3\sigma_{\text{s}}$ and $3\sigma_{\text{s}}$, where $\sigma_{\text{s}}$ is the standard deviation of the time-domain OFDM signal, in order to limit very high peaks, typical for the OFDM signal; a range of $[-3\sigma; 3\sigma]$ encompasses more than 99.7% of the signal distribution, which allows the assumption that the signal generation procedure does not contribute to the non-linear distortion observed in the system; in U-OFDM and eU-OFDM, every information stream is clipped at $[0; 3\sigma]$; 5) root-raised cosine (RRC) pulse shaping with an oversampling factor of 4 and a roll-off factor of 0.1. Note that a single-sided bandwidth of $B = 20$ MHz corresponds to a Nyquist rate, i.e., a double-sided bandwidth of $2B = 40$ MHz, which corresponds to a sampling rate of 160 Msamples/s when the oversampling factor of 4, due to the RRC pulse shaping filter, is taken into account. Then, the subcarrier spacing in this implementation of OFDM is 40 MHz/1024 subcarriers = 20 MHz/512 subcarriers $\approx$ 39 kHz. In the eU-OFDM implementation, the single-sided modulation bandwidth is set to $B = 23$ MHz, the double-sided bandwidth (the Nyquist rate) is $2B = 46$ MHz, the sampling rate is 184 Msamples/s and the subcarrier spacing is $\approx 45$ kHz, respectively.

### B. Signal Processing Techniques

*1) Channel Estimation:* In order to successfully equalize the received information signal, the communication channel has to be known at the receiver. Therefore, a suitable channel estimation technique is required. The received signal is assumed to take the following form:

$$\mathrm{S_r}(f) = \mathrm{H}(f)\mathrm{S_t}(f) + \mathrm{N}(f), \tag{15}$$

where $\mathrm{H}(f)$ denotes the complex channel gain as a function of frequency, $\mathrm{S_t}(f)$ is the frequency component of the transmitted signal, and $\mathrm{N}(f)$ is the realization of the AWGN process at the receiver. The variable $\mathrm{H}(f)$ is assumed to encompass all frequency-dependent attenuation and phase rotation of the information signal from the moment it is generated in the OFDM/U-OFDM/eU-OFDM modulation process at the transmitter up until the moment it is being demodulated at the receiver.

Two estimation techniques have been employed in order to thoroughly characterize the communication channel. In the first technique, multiple copies of an OFDM pilot frame, assumed to be known at the receiver, are transmitted sequentially. The AWGN is zero-mean. Therefore, if $N$ copies of the pilot frame are sent to the receiver, the channel can be estimated with a conventional mean estimator as:

$$\hat{\mathrm{H}}(f) = \frac{\sum_{i=1}^{N} \mathrm{S_r^i}(f)}{N\mathrm{S_t}(f)} = \frac{\sum_{i=1}^{N} \mathrm{H}(f)\mathrm{S_t}(f) + \mathrm{N^i}(f)}{N\mathrm{S_t}(f)}. \tag{16}$$

The noise energy, i.e., the noise variance, can be estimated with a conventional variance estimator as:

$$\hat{\sigma}_{\mathrm{n}}^2(f) = \frac{\sum_{i=1}^{N} \left|\mathrm{S_r^i}(f) - \hat{\mathrm{H}}(f)\mathrm{S_t}(f)\right|^2}{N-1}. \tag{17}$$

For the rest of this paper, this channel and noise estimation technique is referred to as Estimator I. Both the estimated channel gain and the noise variance can be used to estimate the achieved SNR in each frequency band of the communication bandwidth. The estimated SNR can be used to determine how

far the system performance is from a given target BER, and also to identify frequency-dependent distortion effects from background noise and from a non-flat channel response. As a result, modulation on certain subcarriers could be avoided or the modulating symbols could be pre-equalized in order to ensure equivalent performance in all frequency bands that employ the same constellation size. It should be noted that the SNR to which this section refers does not take into account any energy dissipated in the DC component of the information signal. It is different in that sense from the SNR quantities described in Section III. Another notable aspect is the inherent non-linearity of a practical OWC channel. Non-linear distortion occurs in the digital-to-analog/analog-to-digital conversion process, in the transition from an electrical signal to an optical signal at the LED front-end, and in the transition from an optical signal to an electrical signal in the photodetector. The DAC of the AWG and the ADC of the oscilloscope have high precision. The PIN receiver is operated in a range which makes any non-linear distortion from this element negligible. Therefore, the assumption can be made that any significant non-linear distortion in the system is caused by the LED output characteristic. The received time-domain information signal without AWGN can be assumed to be:

$$\hat{\mathrm{s}}_{\mathrm{r}}(t) = \mathrm{h}(t) * \mathrm{z}\left(\mathrm{s}_{\mathrm{t}}(t)\right) \tag{18}$$

where $z(\cdot)$ denotes the non-linear electrical-to-optical conversion at the LED; $[\cdot] * [\cdot]$ is the convolution operator; and $\mathrm{h}(t)$ denotes the impulse response of the communication channel. A time-domain non-linear distortion of an OFDM signal translates into an SNR penalty in the frequency domain [8], [23]. Estimator I is envisioned to work in a linear AWGN channel. If significant non-linear distortion is present in the system, the presented estimator is unable to capture its effect. This occurs because (16) actually estimates:

$$\hat{\mathrm{H}}(f) = \frac{\mathfrak{F}\left\{\hat{\mathrm{s}}_{\mathrm{r}}(t)\right\}}{\mathrm{S}_{\mathrm{t}}(f)} = \frac{\mathrm{H}(f)\mathrm{S}_{\mathrm{t}}(f) + \mathrm{d}(f)}{\mathrm{S}_{\mathrm{t}}(f)} \tag{19}$$

instead of the desired communication channel frequency response $H(f)$. In (19), $\mathfrak{F}\{\cdot\}$ denotes the FFT operation and $\mathrm{d}(f)$ is the frequency-domain representation of the non-linear distortion term. If the non-linear distortion is significant, the distortion term could lead to impaired channel estimation. This effect also compromises the noise variance estimation technique described in (17), because the non-linear distortion term does not contribute to the estimated noise variance. Hence, in high SNR scenarios, where the non-linear distortion limits the performance, the estimated SNR using Estimator I would be inaccurate. As a consequence, a second estimation technique, referred to as Estimator II, is adopted in conjunction with Estimator I. In this technique, multiple different realizations of a pilot frame are sent one after the other instead of the same frame copy being sent multiple times as in Estimator I. Then, the frequency response of the channel is estimated as:

$$\hat{\mathrm{H}}(f) = \frac{1}{N}\sum_{i=1}^{N}\frac{\mathrm{S}_{\mathrm{r}}^{i}(f)}{\mathrm{S}_{\mathrm{t}}^{i}(f)} = \frac{1}{N}\sum_{i=1}^{N}\frac{\mathrm{H}(f)\left(\mathrm{S}_{\mathrm{t}}^{i}(f)+\mathrm{d}^{i}(f)\right)+\mathrm{N}^{i}(f)}{\mathrm{S}_{\mathrm{t}}^{i}(f)}. \tag{20}$$

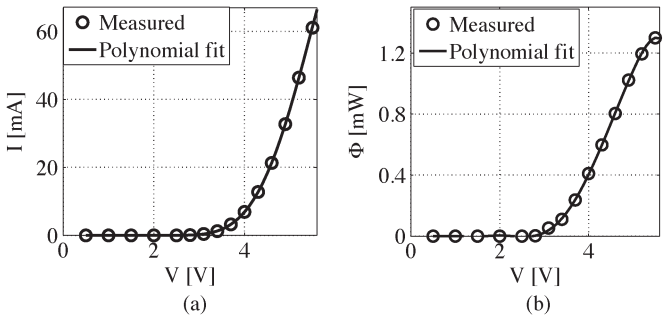


Fig. 10. LED output characteristic. (a) V-I characteristic. (b) V-L characteristic.

It is clear from (20), that in Estimator II both the AWGN and the non-linear distortion are averaged out during the channel estimation. Hence, the channel estimation is more accurate in the presence of non-linear distortion. Furthermore, this technique improves the noise variance estimation because the non-linear distortion term contributes to the sum in (17). In many practical scenarios, where the non-linearity distortion is significant, applying both techniques can be beneficial for evaluating the amount of non-linear distortion in the communication system. This in turn can be helpful in optimizing the active range of the LED. After the channel is estimated with Estimator II, equalization is performed in the frequency domain using a zero-forcing single-tap equalizer.

*2) Non-Linear Distortion:* The main source of non-linear distortion in the presented communication set-up is the output characteristic of the LED. The voltage-to-current (V-I) characteristic of the LED is non-linear as illustrated by the measured data presented in Fig. 10(a). The current-to-light (I-L) characteristic of the LED can be assumed linear for the most part of the device active region. For high current values, however, the light output of the device tends to saturate as the output efficiency of the LED decreases with increasing current density and increasing temperature. As the information signal modulates the voltage over the LED, Fig. 10(b) presents the input-output (voltage-to-light (V-L)) relationship of the LED. The active region of the device starts at around 3V, where the light output begins.

For energy efficiency purposes, the LED should be operated as low as possible in the active region presented in Fig. 10. This part of the region, however, is subjected to significant non-linear distortion as can be inferred from the data in Fig. 10(b). The same conclusion can be made from Fig. 11(a) and Fig. 11(b). In Fig. 11(a), the channel gain for DCO-OFDM estimated with Estimator I exhibits noticeable variation, while the curve computed with Estimator II appears smooth. This is a good indication that the non-linear distortion is significant. The data in Fig. 11(b) leads to the same conclusion because the SNR values on the different subcarriers of DCO-OFDM computed with Estimator II are about 3 dB lower than the SNR values computed with Estimator I.

A non-linear predistortion technique described in [25] was used in order to mitigate the effects of the non-linearity. The technique consists of simply computing the inverse of the

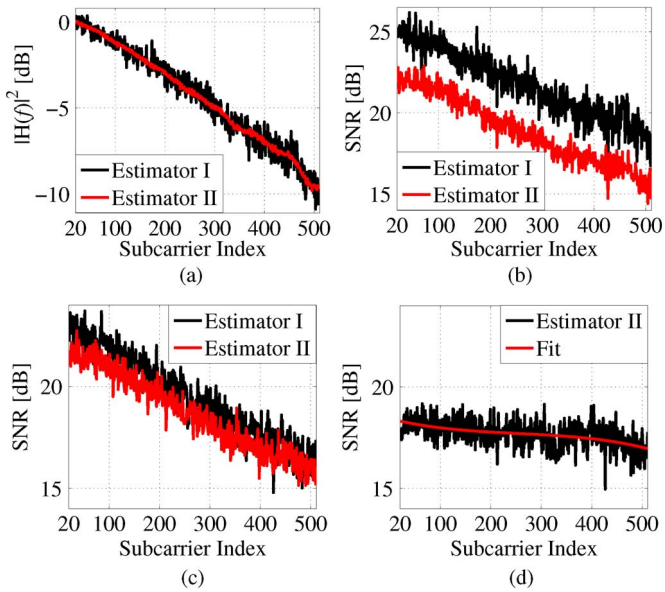


Fig. 11. Communication channel characteristics estimated for an OFDM signal centred at around 3.5 V with a peak-to-peak voltage swing of about 1 V. Subcarriers with indices [0;20] have not been used for communication due to significant DC-wandering effects at the transmitter, caused by AC-coupling in the bias-T. (a) Channel gain. (b) SNR before predistortion. (c) SNR after predistortion. (d) SNR after pre-equalisation.

V-L function presented in Fig. 10(b) and then passing the discrete modulation signal through that inverse function before converting it to an analog signal. The effect of this predistortion technique is illustrated in Fig. 11(c) where the SNR curves estimated with Estimator I and Estimator II are closely adjacent to each other. This suggests that the non-linearity has been significantly reduced. It is interesting to note, however, that the SNR after the predistortion does not appear to be better than the SNR estimated with Estimator II before the predistortion technique. The BER results obtained during the experiments have also confirmed that the predistortion technique does not seem to improve the performance of DCO-OFDM.

However, the predistortion is very beneficial for U-OFDM and eU-OFDM. When no predistortion is applied, both schemes exhibit performance outside the FEC limits. Both U-OFDM and eU-OFDM appear to be more sensitive to non-linear distortion than DCO-OFDM. The effect is likely to arise from the fact that the time-domain information signal in both schemes is concentrated in a more non-linear part of the LED active range compared with the information signal in DCO-OFDM. The higher modulation depths of eU-OFDM are especially vulnerable to this effect because the imperfections in the time-domain signal due to non-linear distortion add up in the demodulation process. When no predistortion is used, U-OFDM and eU-OFDM require significant bias in order to be realized in the relatively linear region of the LED V-L characteristic. This tends to significantly reduce any energy advantage they have over DCO-OFDM. When the predistortion is applied, both U-OFDM and eU-OFDM can be realized with minimum biasing requirements and demonstrate significant energy advantage over DCO-OFDM.

When operated at low current density, i.e., at low bias currents, the LED appears to have a slower frequency response. It is clear from Fig. 11(a) that the frequency response of the LED is not flat. In order to ensure equivalent received SNR levels at all OFDM subcarriers, a pre-equalization technique has been employed. It consists of rescaling the energy allocated to each subcarrier inversely proportional to the SNR values computed with Estimator II and presented in Fig. 11(c). As a result, the achieved SNR profile looks flat as shown in Fig. 11(d).

*3) Estimation of Energy Dissipation:* In order to estimate the average electrical power dissipated at the transmitter front-end, the voltage over the LED is probed and captured with the oscilloscope. Afterwards, the V-I characteristic of the LED is used in order to estimate the current which flows through the device. The average electrical power for each modulation scheme is estimated as:

$$P_{\text{elec}}^{\text{avg}} = \frac{\sum_{n=1}^{N_{\text{total}}} \text{V}[n]\text{I}\left(\text{V}[n]\right)}{N_{\text{total}}}, \tag{21}$$

where $V[n]$ is the $n$th discrete voltage sample captured by the oscilloscope; $\text{I}(\cdot)$ is the V-I characteristic presented in Fig. 10(a); and $N_{\text{total}}$ is the total number of discrete voltage samples captured with the oscilloscope.

In order to compare the optical efficiency of the different modulation schemes, the average irradiance level at the receiver is measured with a commercially available spectral irradiance receiver, Labsphere E1000. The irradiance receiver is positioned in place of the receiver lens. The average irradiance level is measured for each scheme while the LED is being modulated with the respective information signal.

### C. Performance Results

The non-linear relationship between voltage, current and light in the LED, as well as the significant turn-on voltage requirement (almost 3 V), do not allow the simulation results from Section IV to be mapped exactly to the measured results. Nevertheless, the performance trends, derived from the theoretical analysis and the Monte Carlo simulations, can be identified in the results presented in Figs. 12 and 13.

When compared with BPSK eU-OFDM and BPSK DCO-OFDM, 4-QAM U-OFDM is more efficient both in terms of electrical and optical power. The difference to eU-OFDM in terms of both electrical and optical power is approximately 1.5 dB at a BER of $10^{-3}$ and almost 2 dB at a BER of $10^{-4}$. Compared with BPSK DCO-OFDM, 4-QAM U-OFDM requires 3.5 dB less electrical power and 3 dB less optical power for a BER of $10^{-3}$, and it also requires 4 dB less electrical power and 3.5 dB less optical power for a BER of $10^{-4}$. The 16-QAM U-OFDM scheme performs worse than 4-QAM eU-OFDM using approximately equivalent optical power and 1 dB more electrical power at a BER of $10^{-3}$. For a BER of $10^{-4}$, the difference between U-OFDM and eU-OFDM is approximately 3 dB in terms of electrical power and approximately 1 dB in terms of optical power in favour of eU-OFDM. At the same time, 4-QAM DCO-OFDM is approximately 1 dB worse than 4-QAM eU-OFDM in terms of electrical power at a BER of

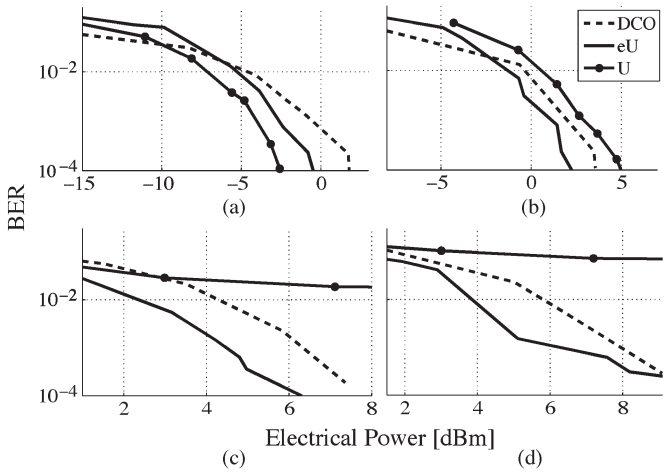


Fig. 12. Performance comparison between eU-OFDM, U-OFDM, and DCO-OFDM for different $M$-QAM constellation sizes as a function of the electrical power dissipated in the LED: (a) BPSK (20 Mb/s). (b) 4-QAM (40 Mb/s). (c) 8-QAM (60 Mb/s). (d) 16-QAM (80 Mb/s). All results have been optimized empirically using exhaustive search experiments.

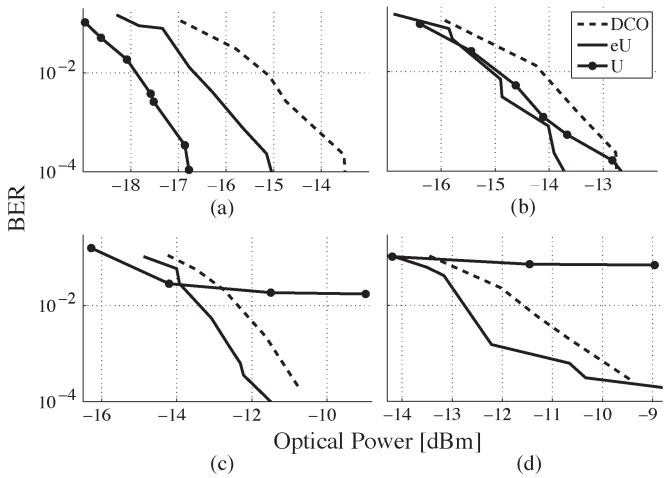


Fig. 13. Performance comparison between eU-OFDM, U-OFDM, and DCO-OFDM for different $M$-QAM constellation sizes as a function of the optical power measured at the receiver: (a) BPSK (20 Mb/s). (b) 4-QAM (40 Mb/s). (c) 8-QAM (60 Mb/s). (d) 16-QAM (80 Mb/s). All results have been optimized empirically using exhaustive search experiments.

$10^{-3}$ and 2 dB worse at a BER of $10^{-4}$. In terms of optical power, DCO-OFDM is 0.7 dB worse at a BER of $10^{-3}$ and 1 dB worse at a BER of $10^{-4}$ when compared to eU-OFDM. The non-linear distortion introduces a noticeable effect on the 16-QAM U-OFDM signal and the corresponding curves in Figs. 12(b) and 13(b) exhibit a noticeable change in slope for a BER lower than $10^{-3}$. In Fig. 12(c), 8-QAM eU-OFDM exhibits a 2 dB improvement over DCO-OFDM in electrical power dissipation for a BER of $10^{-3}$ and a BER of $10^{-4}$. At the same time, the optical power requirement of 8-QAM eU-OFDM is approximately 1 dB less than the optical power requirement of 8-QAM DCO-OFDM for both a BER of $10^{-3}$ and a BER of $10^{-4}$. The U-OFDM scheme with a constellation size of $M \geq 64$ could not be realized within the FEC BER due to the non-linear distortion. The non-linear predistortion procedure does not appear to be beneficial when the information signal has values higher than $\approx 4.5$ V. This could be explained by the fact that the non-linearity in the upper part of the LED active region is not memoryless and a more complicated predistortion procedure, like the one described in [26], should be applied. For 16-QAM, eU-OFDM is again more efficient than DCO-OFDM with 2 dB of electrical power improvement and 1.5 dB of optical power improvement at a BER of $10^{-3}$. At a BER close to $10^{-4}$, the non-linear distortion affects the eU-OFDM scheme significantly and it requires approximately the same electrical and optical power as 16-QAM DCO-OFDM. For higher $M$-QAM constellation sizes, eU-OFDM could not be realized within the FEC limits due to the non-linearity.

Non-linear distortion caused by the LED output characteristic proves to be the limiting factor for eU-OFDM implementation in an OWC system. The memoryless predistortion technique presented in Section V-B2 seems to mitigate the distortion effects of the non-linear V-I relationship. In a future implementation, this issue could be avoided by substituting the presented voltage modulator of the LED with a current modulating circuit. The drop in output efficiency of the LED could be reduced with appropriate heat-sinking techniques. Furthermore, the issue of efficiency dropping in LEDs for higher current densities suggests that energy-efficient implementations, both for communication and illumination applications, are likely to benefit from a system configuration with multiple LEDs operated in parallel at the lower end of their active region. This could resolve the non-linearity issue for eU-OFDM as it would allow the light signal levels to scale linearly with the number of output devices without further non-linear effects.

## VI. Conclusion

This work presents a novel modulation technique, eU-OFDM, which allows a unipolar real OFDM signal to be realized without significant loss of spectral efficiency compared to similar state-of-the-art techniques. Monte Carlo simulation results and the theoretical analysis confirm that eU-OFDM promises to deliver very significant energy savings compared to other OFDM-based modulation schemes, particularly in high spectral efficiency configurations. The improved performance is enabled at a cost of higher computational complexity in the signal generation and signal demodulation procedures. This complexity, however, does not appear to be prohibitive for practical implementations of eU-OFDM.

A proof-of-concept experimental set-up has been designed for eU-OFDM and for its more basic variant of U-OFDM. Results indicate that both techniques are practically feasible and tend to deliver the expected energy efficiency. Non-linear distortion has proven to be the most significant limitation for U-OFDM/eU-OFDM realization in an OWC system. Techniques for mitigation of the non-linear distortion, such as signal predistortion, can alleviate this and can enable the required performance by both schemes. Future work on reducing non-linear distortion by applying improved predistortion techniques and by improving the linearity of the transmitter front-end device is expected to enable even higher performance results from eU-OFDM.

## REFERENCES


[1] Cisco Visual Networking Index, "Global mobile data traffic forecast update, 2014–2019," Cisco, San Jose, CA, USA, White Paper, Feb. 2015. [Online]. Available: http://www.cisco.com/c/en/us/solutions/collateral/service-provider/visual-networking-index-vni/white_paper_c11-520862.pdf

[2] H. Elgala, R. Mesleh, and H. Haas, "Indoor optical wireless communication: Potential and state-of-the-art," *IEEE Commun. Mag.*, vol. 49, no. 9, pp. 56–62, Sep. 2011.

[3] H. Burchardt, N. Serafimovski, D. Tsonev, S. Videv, and H. Haas, "VLC: Beyond point-to-point communication," *IEEE Commun. Mag.*, vol. 52, no. 7, pp. 98–105, Jul. 2014.

[4] A. M. Khalid, G. Cossu, R. Corsini, P. Choudhury, and E. Ciaramella, "1-Gb/s transmission over a phosphorescent white LED by using rate-adaptive discrete multitone modulation," *IEEE Photon. J.*, vol. 4, no. 5, pp. 1465–1473, Oct. 2012.

[5] G. Cossu, A. M. Khalid, P. Choudhury, R. Corsini, and E. Ciaramella, "3.4 Gbit/s visible optical wireless transmission based on RGB LED," *Opt. Exp.*, vol. 20, no. 26, pp. B501–B506, Dec. 2012.

[6] D. Tsonev *et al.*, "A 3-Gb/s single-LED OFDM-based wireless VLC link using a gallium nitride $\mu$LED," *IEEE Photon. Technol. Lett.*, vol. 26, no. 7, pp. 637–640, Apr. 2014.

[7] J. B. Carruthers and J. M. Kahn, "Multiple-subcarrier modulation for nondirected wireless infrared communication," *IEEE J. Sel. Areas Commun.*, vol. 14, no. 3, pp. 538–546, Apr. 1996.

[8] D. Tsonev, S. Sinanovic, and H. Haas, "Complete modeling of nonlinear distortion in OFDM-based optical wireless communication," *J. Lightw. Technol.*, vol. 31, no. 18, pp. 3064–3076, Sep. 15 2013.

[9] J. Armstrong and A. Lowery, "Power efficient optical OFDM," *Electron. Lett.*, vol. 42, no. 6, pp. 370–372, Mar. 16, 2006.

[10] S. C. J. Lee, S. Randel, F. Breyer, and A. M. J. Koonen, "PAM-DMT for intensity-modulated and direct-detection optical communication systems," *IEEE Photon. Technol. Lett.*, vol. 21, no. 23, pp. 1749–1751, Dec. 2009.

[11] D. Tsonev, S. Sinanović, and H. Haas, "Novel unipolar orthogonal frequency division multiplexing (U-OFDM) for optical wireless," in *Proc. IEEE VTC Spring*, Yokohama, Japan, May 6–9, 2012, pp. 1–5.

[12] N. Fernando, Y. Hong, and E. Viterbo, "Flip-OFDM for optical wireless communications," in *Proc. IEEE ITW*, Paraty, Brazil, Oct. 16–20, 2011, pp. 5–9.

[13] S. Dimitrov, S. Sinanovic, and H. Haas, "A comparison of OFDM-based modulation schemes for OWC with clipping distortion," in *Proc. IEEE GC Wkshps*, Houston, TX, USA, Dec. 5–9, 2011, pp. 787–791.

[14] S. Dissanayake, K. Panta, and J. Armstrong, "A novel technique to simultaneously transmit ACO-OFDM and DCO-OFDM in IM/DD systems," in *Proc. IEEE GC Wkshps*, Houston, TX, USA, Dec. 5–9, 2011, pp. 782–786.

[15] K. Asadzadeh, A. Farid, and S. Hranilovic, "Spectrally factorized optical OFDM," in *Proc. 12th CWIT*, May 17–20, 2011, pp. 102–105.

[16] J. Armstrong and B. J. C. Schmidt, "Comparison of asymmetrically clipped optical OFDM and DC-biased optical OFDM in AWGN," *IEEE Commun. Lett.*, vol. 12, no. 5, pp. 343–345, May 2008.

[17] S. Dimitrov, S. Sinanovic, and H. Haas, "Signal shaping and modulation for optical wireless communication," *J. Lightw. Technol.*, vol. 30, no. 9, pp. 1319–1328, May 2012.

[18] S. Dimitrov, S. Sinanovic, and H. Haas, "Clipping noise in OFDM-based optical wireless communication systems," *IEEE Trans. Commun.*, vol. 60, no. 4, pp. 1072–1081, Apr. 2012.

[19] F. Xiong, *Digital Modulation Techniques*, 2nd ed. Norwood, MA, USA: Artech House, 2006.

[20] D. Tsonev, S. Sinanović, and H. Haas, "Enhanced subcarrier index modulation (SIM) OFDM," in *Proc. IEEE GC Wkshps*, Houston, TX, USA, Dec. 5–9, 2011, pp. 728–732.

[21] Z. Yu, R. Baxley, and G. Zhou, "Peak-to-average power ratio and illumination-to-communication efficiency considerations in visible light OFDM systems," in *Proc. IEEE ICASSP*, Vancouver, BC, Canada, May 26–31, 2013, pp. 5397–5401.

[22] ITU-T, "Forward error correction for high bit-rate DWDM submarine systems," Geneva, Switzerland, Tech. Rep. ITU-T G.975.1, 2004. Retrieved Nov. 19, 2013. [Online]. Available: http://www.itu.int/rec/T-REC-G.975.1-200402-I/en

[23] S. Dimitrov and H. Haas, "Information rate of OFDM-based optical wireless communication systems with nonlinear distortion," *J. Lightw. Technol.*, vol. 31, no. 6, pp. 918–929, Mar. 15, 2013.

[24] D. Tsonev, S. Sinanović, and H. Haas, "Pulse shaping in unipolar OFDM-based modulation schemes," in *Proc. IEEE GLOBECOM Workshop*, Anaheim, CA, USA, Dec. 3–7, 2012, pp. 1208–1212.

[25] H. Elgala, R. Mesleh, and H. Haas, "Non-linearity effects and predistortion in optical OFDM wireless transmission using LEDs," *Int. J. Ultra Wideband Commun. Syst.*, vol. 1, no. 2, pp. 143–150, 2009.

[26] T. Kamalakis, J. Walewski, G. Ntogari, and G. Mileounis, "Empirical Volterra-series modeling of commercial light-emitting diodes," *J. Lightw. Technol.*, vol. 29, no. 14, pp. 2146–2155, Jul. 2011.


**Dobroslav Tsonev** (S'12–M'13) received the B.Sc. degree in electrical engineering and computer science in 2008 from Jacobs University Bremen, Bremen, Germany, and the M.Sc. degree in communication engineering with a specialisation in electronics in 2010 from the Munich Institute of Technology, Munich, Germany. Currently, he is pursuing the Ph.D. degree in electrical engineering at the University of Edinburgh. His main research interests lie in the area of optical wireless communications with an emphasis on visible light communications.

**Stefan Videv** received the B.Sc. degree in electrical engineering and computer science and the M.Sc. degree in communications, systems and electronics from Jacobs University, Bremen, Germany, in 2007 and 2009, respectively, and the Ph.D. degree for his thesis titled "Techniques for Green Radio Cellular Communications" from the University of Edinburgh, in 2013. He is currently employed as an Experimental Officer at the Li-Fi R&D Center, University of Edinburgh and working in the field of visible light communications (VLC). His research focus at the moment is on quick prototyping of communication systems, smart resource allocation, and energy efficient communications.

**Harald Haas** (S'98–A'00–M'03) received the Ph.D. degree from the University of Edinburgh, in 2001. He currently holds the Chair of Mobile Communications at the University of Edinburgh. His main research interests are in optical wireless communications, hybrid optical wireless and RF communications, spatial modulation, and interference coordination in wireless networks. He first introduced and coined spatial modulation and 'Li-Fi'. Li-Fi was listed among the 50 best inventions in *TIME Magazine* 2011. He was an invited speaker at TED Global 2011, and his talk has been watched online more than 1.5 million times. He is Co-founder and Chief Scientific Officer (CSO) of pureLiFi Ltd. He holds 31 patents and has more than 30 pending patent applications. He has published 300 conference and journal papers including a paper in *Science*. He was co-recipient of a best paper award at the IEEE Vehicular Technology Conference in Las Vegas, NV, USA, in 2013. In 2012, he was the only recipient of the prestigious Established Career Fellowship from the Engineering and Physical Sciences Research Council (EPSRC) within Information and Communications Technology in the U.K. He is recipient of the Tam Dalyell Prize 2013 awarded by the University of Edinburgh for excellence in engaging the public with science. In 2014, he was selected by EPSRC as one of ten Recognising Inspirational Scientists and Engineers (RISE) Leaders.